Hydrophobic Loop Dynamics and Actin Filament Stability†

Damon Scoville,‡ John D. Stamm,§,|| Dora Toledo-Warshaviak,‡,§ Christian Altenbach,§ Martin Phillips,‡ Alexander Shvetsov,‡ Peter A. Rubenstein,⊥ Wayne L. Hubbell,‡,§ and Emil Reisler*,‡

Department of Chemistry and Biochemistry and Molecular Biology Institute, University of California, Los Angeles, California 90095, Department of Biochemistry, University of Iowa College of Medicine, Iowa City, Iowa 52242, and Jules Stein Eye Institute and Department of Chemistry and Biochemistry, University of California, Los Angeles, California 90095

Received June 20, 2006; Revised Manuscript Received September 1, 2006

ABSTRACT: It has been postulated that the hydrophobic loop of actin (residues 262−274) swings out and inserts into the opposite strand in the filament, stabilizing the filament structure. Here, we analyzed the hydrophobic loop dynamics utilizing four mutants that have cysteine residues introduced at a single location along the yeast actin loop. Lateral, copper-catalyzed disulfide cross-linking of the mutant cysteine residues to the native C374 in the neighboring strand within the filament was fastest for S265C, followed by V266C, L267C, and then L269C. Site-directed spin labeling (SDSL) studies revealed that C265 lies closest to C374 within the filament, followed by C266, C267, and then C269. These results are not predicted by the Holmes extended loop model of F-actin. Furthermore, we find that disulfide cross-linking destroys L267C and L269C filaments; only small filaments are observed via electron microscopy. Conversely, phalloidin protects the L267C and L269C filaments and inhibits their disulfide cross-linking. Combined, our data indicate that, in solution, the loop resides predominantly in a "parked" position within the filament but is able to dynamically populate other conformational states which stabilize or destabilize the filament. Such states may be exploited within a cell by filament-stabilizing and -destabilizing factors.

Actin filaments play a key role in force generation in muscle cells and in many processes within non-muscle cells. Actin interacts with more than 150 proteins (*1*), and a detailed understanding of its conformational states in the globular (G-actin)[1] and filamentous (F-actin) forms is critical to a comprehensive description of its interactions with these proteins and its role in cellular processes. The 1990 Holmes model of F-actin (*2*) is the prevailing representation of the actin filament. In this model, the hydrophobic loop (residues 262−274) is postulated to swing out and insert into the neighboring strand in a hydrophobic pocket between two actin protomers, thereby stabilizing the filament. Recent studies showed that the mobility of the hydrophobic loop is indeed necessary for filament stability; when the loop was locked by intramolecular disulfide bond formation to the monomer backbone in the L180C/L269C/C374A yeast actin mutant, filaments did not form, even in the presence of the actin-stabilizing agent phalloidin (*3*). Also, locking the loop after filament formation caused filament destruction (*4*).

Feng et al. (*5*) first used the yeast actin loop mutant S265C to gain insight into changes occurring during actin polymerization. An excimer band was formed in F-actin when pyrene probes were attached to actin residues 265 and 374, indicating the residues in separate protomers were within 18 Å of one another in the filament. In addition, pyrene emission spectra of C265- and C374-labeled actin revealed polymerization-related conformational changes in the 262−274 loop and the C-terminus of F-actin. Furthermore, fluorescence changes at position 265 were also noted when myosin S1 was bound to the labeled actin, indicating that changes in subdomains 1 and 2 were transmitted throughout subdomains 3 and 4.

Musib et al. (*6*) subsequently reported fluorescence changes for pyrene maleimide and acrylodan attached at other hydrophobic loop residues mutated to cysteines (266, 267, and 269) due to actin polymerization. These changes suggested that the loop residues "sampled" multiple environments in the F-actin state. Moreover, a pyrene excimer band was observed in F-actin with labels at residues 266 and 374, positioning them within 18 Å of each other, and indicating the loop was in a parked position. As argued by these authors, the two bulky succinimidyl pyrene moieties could not be accommodated in F-actin with the loop extended, as suggested by the Holmes model.

Kim et al. (*7*) provided further insight into the dynamics of F-actin and loop 262−274 by employing disulfide cross-linking reactions to impose constraints upon F-actin structure. Although models of F-actin predicted distances of 18−20

† This work was supported by grants from the U.S. Public Health Service (GM 077190) and the National Science Foundation (MCB 0316269) to E.R., from the U.S. Public Health Service (GM 33689) to P.A.R., from the U.S. Public Health Service (EY 05216) and Jules Stein Professor Endowment to W.L.H., and from the U.S. Public Health Service (Training Grant T32 EY07026) to J.D.S.

* To whom correspondence should be addressed: 405 Hilgard Ave., UCLA, MBI Rm. 401, Los Angeles, CA 90095. Telephone: (310) 825-2668. Fax: (310) 206-7286. E-mail: reisler@mbi.ucla.edu.

‡ Department of Chemistry and Biochemistry and Molecular Biology Institute, University of California.

§ Jules Stein Eye Institute and Department of Chemistry and Biochemistry, University of California.

|| Present address: Department of Physics, University of Evansville, Evansville, IN 47722.

⊥ University of Iowa College of Medicine.

[1] Abbreviations: G-actin, globular or monomeric actin; F-actin, filamentous actin; DTT, dithiothreitol; RhPh, rhodamine-labeled phalloidin; SDSL, site-directed spin labeling; EM, electron microscopy.

10.1021/bi061229f CCC: $33.50
Published on Web 10/20/2006

Å between residues 265 and 374, 41 and 374, and 41 and 265, disulfide cross-links were formed in cysteine mutants in F-actin and the cross-linked filaments appeared normal in electron microscopy observations. These experiments demonstrated the inherent flexibility of the actin structure at the C-terminus, DNaseI binding loop, and hydrophobic loop sites and posed an interesting question regarding the permissible states of loop 262−274 in F-actin.

This work extends the probing of hydrophobic loop dynamics by using the loop cysteine mutants to map the dynamic and conformational space available to loop residues in G- and F-actin. To this end, we have utilized site-directed spin labeling in conjunction with disulfide cross-linking and electron microscopy studies to obtain a more detailed and better understanding of hydrophobic loop dynamics within the actin filament and the loop states that support the filament structure.

MATERIALS AND METHODS

Yeast Actin Mutants. Yeast actin mutant strains S265C, S265C/C374A, V266C, V266C/C374A, L267C, L267C/C374A, L269C, and L269C/C374A were described previously (*6*).

Protein Purification. Yeast actin was purified by affinity chromatography on a DNaseI column as described by Shvetsov et al. (*3*). The purified G-actin was stored on ice, in Tris-HCl (pH 8.0), 1.0 mM DTT, 0.2 mM ATP, and 0.2 mM $CaCl_2$. Fresh DTT was added daily. For all experiments, and to remove DTT, G-actin was passed through a Sephadex G-50 column equilibrated with 10 mM MOPS (pH 7.4), 0.2 mM ATP, and 0.2 mM $CaCl_2$.

Disulfide Cross-Linking Experiments. G-Actin (10 μM) was polymerized in the presence of 2.0 mM $MgCl_2$, 0.2 mM ATP, 0.2 mM $CaCl_2$, and 10 mM MOPS (pH 7.4) for at least 20 min at room temperature. When present, phalloidin was added to the polymerized actin in a 1:1 ratio with actin and allowed to equilibrate for 10 min prior to actin cross-linking. $CuSO_4$ (5.0−15 μM) was then added to catalyze disulfide cross-linking at room temperature. Time point aliquots were taken directly before the addition of $CuSO_4$ (zero time point) and 5, 30, 60, 90, and 120 min after the addition of $CuSO_4$. Reactions were stopped with excess (2.0 mM) *N*-ethylmaleimide (NEM), which blocks unreacted cysteine groups. Time point samples were run on SDS−PAGE gels under nonreducing conditions and stained with Coomassie blue for visualization. Gels were scanned, and density values of monomer bands were obtained using SigmaGel version 1.0 (Jandel Scientific, San Rafael, CA). Data were then analyzed and plotted in Sigma Plot 2000 version 6.0 (SPSS, Inc., Chicago, IL).

Light Scattering Experiments. Actin polymerization, disulfide cross-linking, and disulfide reduction were monitored by light scattering measurements (at 350 nm) using a Photon Technology International (PTI, Lawrenceville, NJ) spectrofluorimeter and FeliX32 Analysis version 1.1 (PTI). G-Actin (10 μM) was polymerized as described above. $CuSO_4$ (20−30 μM) was then added to catalyze disulfide cross-linking at room temperature. To accelerate the reactions, higher concentrations (20−30 μM) of $CuSO_4$ were added for light scattering experiments than for kinetics experiments.

Rhodamine-Labeled Phalloidin Binding Experiments. G-Actin (10 μM) was polymerized as described above. F-Actin (5.0 μM) was disulfide cross-linked at room temperature for at least 1 h in the presence of $CuSO_4$ (20−30 μM). Rhodamine-labeled phalloidin (RhPh), at a concentration of 50 nM, was then added at a 1:100 RhPh:actin ratio to cross-linked and un-cross-linked filaments. The solution was mixed quickly, and binding was monitored through changes in RhPh fluorescence. RhPh was excited at 554 nm, and the emission was monitored at 573 nm. Data were recorded as described in Light Scattering Experiments.

Electron Microscopy. Mutant yeast actin (10 μM) was polymerized as described above in the presence or absence of DTT (5.0 mM) for 20 min at 25 °C. For disulfide cross-linking, 20−30 μM $CuSO_4$ was added to F-actin and the reaction was allowed to proceed for 1 h at room temperature. For cross-link reversal, DTT was added to the cross-linked samples to a final concentration of 5.0 mM. Samples were then incubated for 1 h or overnight at room temperature or 4 °C, respectively. To adsorb actin to carbon-coated holey grids, actin was diluted to 2.5 μM, adsorbed to grids, and negatively stained with 1% uranyl acetate. Grids were observed using a Hitachi H7000 electron microscope at 31200× magnification.

Pelleting Assays. Actin (10 μM) was polymerized and cross-linked as described above. For uncross-linked samples, 2.0 mM DTT was added to the solution and the actin was incubated for 1 h at room temperature. NEM (2.0 mM) was added to the cross-linked samples to block free cysteine residues. The samples were then centrifuged at 360000*g* for 30 min at 4 °C in a Beckman TLA-100 rotor. The supernatants and pellets were adjusted to the same volumes and analyzed by SDS−PAGE.

Site-Directed Spin Labeling. Yeast single and double mutant G-actin was passed through Sephadex G-50 columns equilibrated with 10 mM MOPS (pH 7.4), 0.2 mM ATP, and 0.2 mM $CaCl_2$. G-Actin was then incubated for 1 h at room temperature in the same buffer containing a 3-fold molar excess (over actin) of a spin labeling reagent [MTSL, (1-oxy-2,2,5,5-tetramethylpyrrolinyl-3-methyl)methanethiosulfonate] that reacts with cysteine residues to generate the side chain, designated R1 (*8*). For distance measurements, actin was labeled with either pure spin-labeled reagent (MTSL) or a 1:3 (molar ratio) mixture of MTSL with a diamagnetic analogue [(1-methoxy-2,2,5,5-tetramethylpyrrolinyl-3-methyl)methanethiosulfonate], according to the method described in ref *8*. Both reagents were kindly provided by Kálmán Hideg (University of Pécs, Pécs, Hungary). Previous work has shown that other nonreactive cysteines present in the actin sequence are not labeled under conditions employed in this work (*9*). Actin was again passed through Sephadex G-50 columns to remove any unreacted label and was then concentrated to 30 μM using Vivaspin 0.5 mL concentrators (Viva Science, Hannover, Germany) with a 10 000 molecular weight cutoff PES membrane. Samples of freshly spin-labeled G-actin were polymerized for at least 20 min at room temperature with 2.0 mM $MgCl_2$. Spectra of G- and F-actin were recorded at X-band using either a Bruker E580 spectrometer and a cavity (4119HS) or a Varian 109 spectrometer fitted with a loop gap resonator (*10*). Labeled actin was analyzed in a Suprasil flat cell (volume of 40 μL; Wilmad, Buena, NJ) or a glass capillary (volume of 5.0 μL; VitroCom, Inc., Mountain Lakes, NJ) in each spectrometer, respectively. Each spectrum was collected

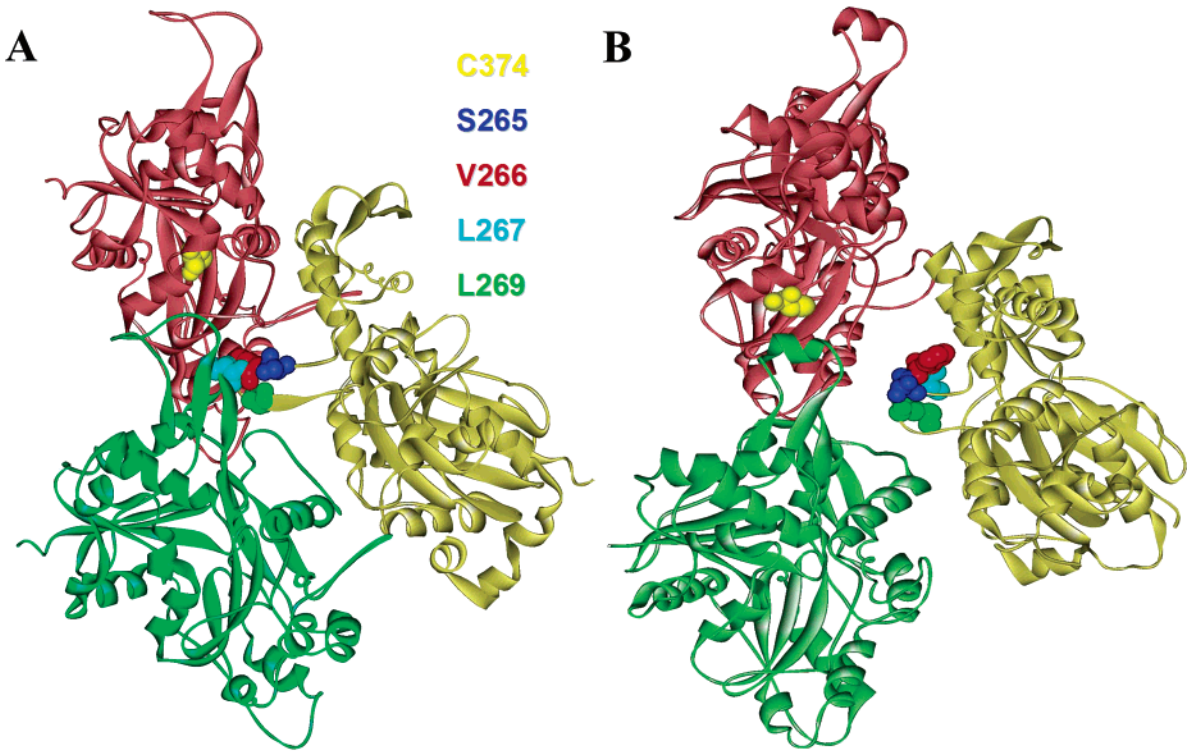

FIGURE 1: Holmes model of the actin filament shown with the hydrophobic loop extended (A) or parked (B), and pertinent residues highlighted. Residues colored yellow represent the native C374, to which cysteine mutants generated in the loop will be disulfide cross-linked in F-actin. S265 is colored blue, V266 red, L267 cyan, and L269 green. Individual actin protomers are distinguished by their ribbon color. This figure was generated utilizing WebLab ViewerPro version 4.0.

with a 30 s scan time, a 160 G field scan, a modulation amplitude of 4.0 G at 100 kHz, and an incident microwave power of either 10 mW (4119HS) or 2.0 mW (loop gap), as in ref *9*. The recorded data are averages of 20−60 scans and are trimmed to 100 G for display.

Measurement of Interspin Distances. Altenbach et al. (*8*) showed that distances between two spin-labels can be determined at room temperature using rigid lattice theory in cases where the overall rotational correlation time of the protein, and thus of the interspin vector, is slow. Briefly, the EPR spectrum of a molecule with an interacting pair of R1 side chains is assumed to be a convolution of the spectrum with no spin−spin interactions (noninteracting) (*11*) with a weighted sum of Pake functions (*12*), and the distance distribution is calculated from the known distance dependence of the Pake functions using software written in LabVIEW (National Instruments) (*8*).

MTSL or a 1:3 mixture of MTSL and a diamagnetic analogue was used as described above to obtain the interacting or noninteracting spectra, respectively (*8*).

RESULTS

The purpose of this work has been to better understand the relationship between actin filament dynamics and the hydrophobic loop topography by applying constraints on the conformational states of this loop. Specifically, we have used cysteine mutants S265C, V266C, L267C, and L269C (Figure 1) in the hydrophobic loop and the native C374 in the C-terminus for cross-linking experiments in yeast actin. In addition, we used these mutants to observe the local dynamics at the loop sites and the distances from these sites to C374 on the neighboring strand.

Kinetics of Disulfide Cross-Linking of Loop Cysteines to C374 in F-Actin. Copper-catalyzed disulfide formation with C374 proceeded at different rates with the four loop cysteine mutants and required different amounts of $CuSO_4$ to produce similar reaction progress. S265C cross-linked faster [$(1.3 \pm 0.6) \times 10^{-2}$ s^{-1}] than V266C (4.1×10^{-3} s^{-1}) (Figure 2A) in the presence of 5.0 μM $CuSO_4$, while 15 μM $CuSO_4$ was needed for efficient cross-linking of L267C [$(2.2 \pm 0.7) \times 10^{-2}$ s^{-1}] and L269C ($4.3 \times 10^{-2} \pm 0.5 \times 10^{-1}$ s^{-1}). $CuSO_4$ (10 μM) was normally used for efficient V266C cross-linking ($5.4 \times 10^{-2} \pm 0.9 \times 10^{-1}$ s^{-1}). L267C and L269C exhibited almost no cross-linking in the presence of 5.0 μM $CuSO_4$ over the same time scale (data not shown). This trend, with S265C cross-linking the fastest, is inconsistent with the extended loop Holmes model in which L267 lies closest to C374 within the filament, followed by V266, S265, and then L269. The disulfide cross-linking data indicate a different ordering of the hydrophobic loop residues, with S265 being closest to C374, followed by V266, L267, and L269. This order may be a reflection of real, different average proximities of loop residues to C374 and/or their different mobilities, and thus the frequency at which they approach C374. The SDSL experiments reported below support the proximity basis of the order given above but reveal also a possible effect of residue mobility on the measured rates of cross-linking.

We decided to test the disulfide cross-linking of the four mutants in the presence of phalloidin, an F-actin-stabilizing agent (*13*). In S265C, cross-linking is accelerated in the presence of phalloidin (Figure 2C). Interestingly, phalloidin exhibits a strong inhibitory effect in L269C (Figure 2B,C), the opposite of what is observed in S265C. V266C presents

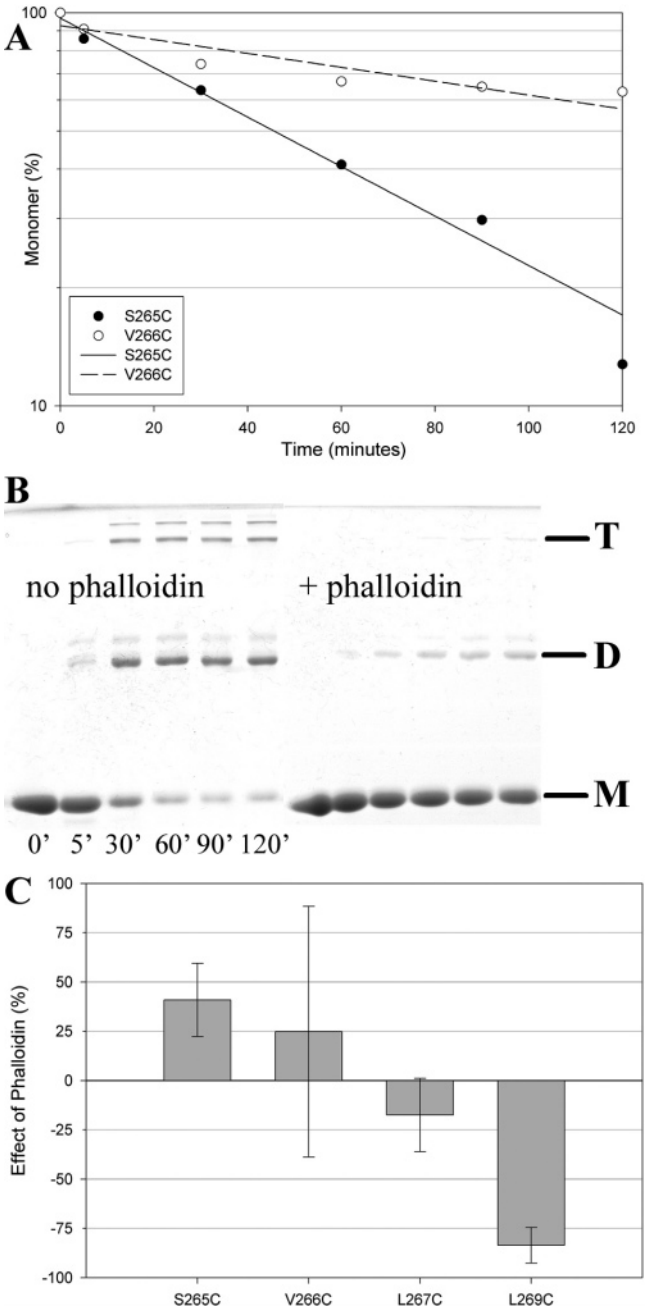

FIGURE 2: Disulfide cross-linking kinetic experiments in yeast mutant F-actin. (A) S265C and V266C cross-linking in the presence of 5.0 μM $CuSO_4$. Black circles (●) depict S265C and white circles (○) V266C disulfide cross-linking time points. (B) SDS−PAGE of L269C cross-linked in the absence and presence of an equimolar amount of phalloidin (15 μM $CuSO_4$). (C) Bar chart illustrating the effect of phalloidin in percentage increase or decrease in the rates of disulfide cross-linking in yeast actin mutants. Error bars represent the standard error. Disulfide cross-linking rates increased by 41 and 25% for S265C and V266C, respectively, and decreased by 17 and 84% for L267C and L269C, respectively. Percentage changes were calculated from the observed rate constants.

a slight acceleration, whereas L267C exhibits a slight decrease in the rate of cross-linking (Figure 2C). Thus, a distinct trend and transition is observed in the residues of the hydrophobic loop when cross-linked in the presence of phalloidin, namely, from the acceleration of the reaction to its inhibition. Also, it was impossible to fully cross-link L267C or L269C filaments in the presence of phalloidin, while the reaction with S265C and V266C proceeded well (data not shown).

Electron Microscopy. The difference in the rates of disulfide cross-linking of C374 to C265 and C266 versus C267 and C269 in F-actin prompted the electron microscopic (EM) examination of the cross-linked filaments (Figure 3). As published previously (*7*), S265C disulfide cross-linked filaments appeared normal under EM (data not shown). Cross-linked V266C F-actin also exhibits a relatively normal morphology, with perhaps slightly kinked filaments (Figure 3B). However, cross-linking of L267C and L269C destabilizes F-actin (Figure 3D,H); only few and short filaments are observed in such samples, while the unoxidized filaments appear normal (Figure 3C,G). The destabilization of the filaments could also be inhibited with the presence of equimolar phalloidin during the cross-linking (Figure 3F,J). The cross-linking-induced disruption of L267C and L269C filaments could be reversed by disulfide reduction with 1.0−5.0 mM DTT (Figure 3E,I); however, this recovery process was relatively slow (>1 h) compared to the cross-linking time (≤1 h).

Solution Tests of Actin Filaments. To confirm electron microscopy observations, the polymerization state of the four uncross-linked (data not shown) and cross-linked cysteine loop mutants was checked in pelleting experiments (Figure 4). S265C and V266C (Figure 4A,B) disulfide cross-linked filaments were pelleted completely in such assays (30 min at 360000*g*), while the cross-linked L267C and L269C actin was found only in the supernatant (Figure 4C,D). This indicates either depolymerization or breakdown of L267C and L269C F-actin into very short filaments. In the unoxidized form, all four mutant F-actin samples were pelleted readily, with the L267C and L269C actins exhibiting a small fraction of the protein in the supernatant.

Filament disruption upon disulfide cross-linking of L267C and L269C F-actin was monitored by light scattering measurements. As shown in Figure 5, both L267C and L269C G-actin are polymerized rapidly upon addition of $MgCl_2$ (Figure 5, arrows). In both cases, the initiation of cross-linking with the addition of $CuSO_4$ (Figure 5, arrowheads) results in a light scattering decrease, indicating filament depolymerization. This process appears much faster in L269C than in L267C actin. Actin depolymerization can be reversed with the addition of 1.0 mM DTT (Figure 5, stars). Importantly, S265C and V266C F-actin did not exhibit any significant light scattering changes upon their copper-catalyzed disulfide cross-linking and subsequent reduction of disulfide with DTT (data not shown). This confirms the results of pelleting and EM experiments showing little, if any, effect of disulfide cross-linking on these filaments.

As a further test of actin filament features, we observed the binding of rhodamine-labeled phalloidin (RhPh) to F-actin. S265C and V266C cross-linked and uncross-linked filaments bound RhPh equally well, with a similar rate constant (Figure 6). However, cross-linking of L267C caused a 2-fold decrease in the binding rate of RhPh (Figure 6), while cross-linked L269C did not appear to bind RhPh at all (data not shown). The partial or complete inhibition of binding of RhPh to cross-linked L267C and L269C most likely reflects the absence of normal numbers and size of actin filaments in these mutants, as well as the ability of the cross-link to hinder the "structural breathing" that would

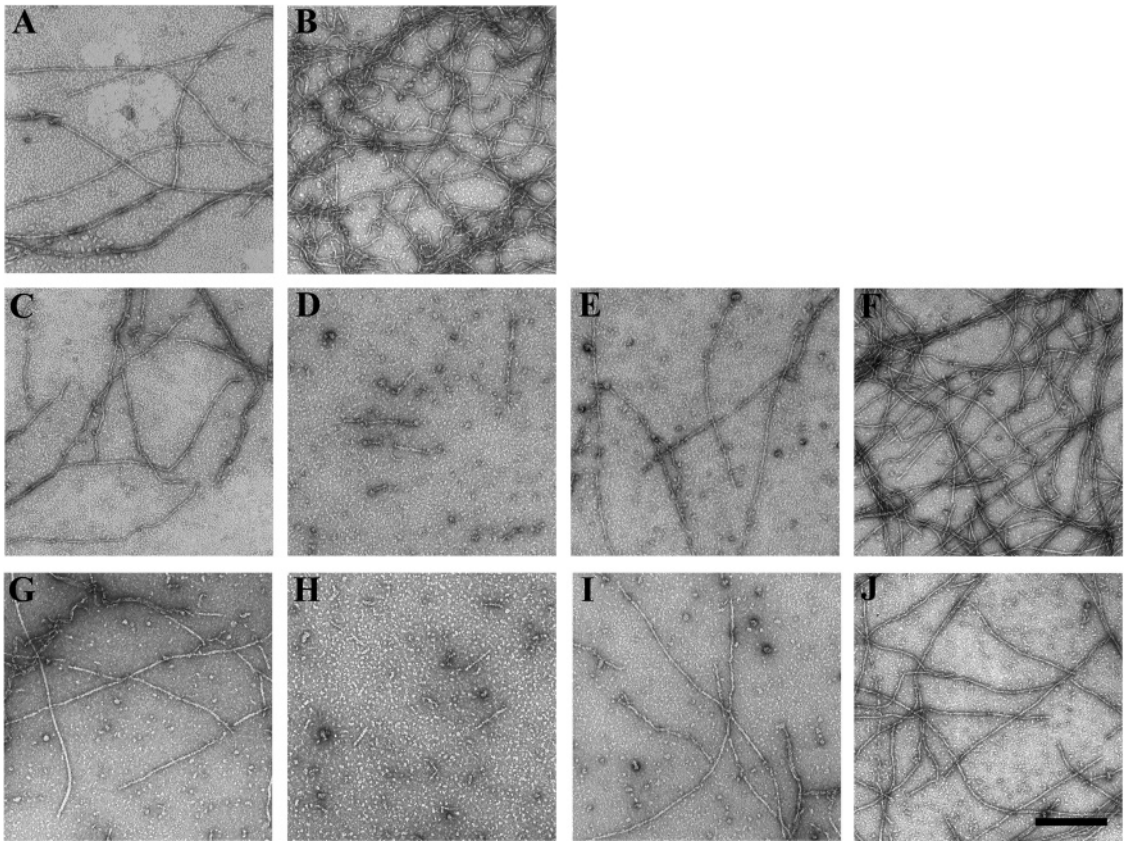

FIGURE 3: Electron microscopy images of (A) V266C F-actin, (B) V266C disulfide-cross-linked F-actin, (C) L267C F-actin, (D) L267C disulfide cross-linked F-actin, (E) L267C disulfide cross-linked F-actin 1 h after addition of 1.0−5.0 mM DTT, (F) L267C disulfide cross-linked F-actin in the presence of an equimolar amount of phalloidin, (G) L269C F-actin, (H) L269C disulfide cross-linked F-actin, (I) L269C disulfide cross-linked F-actin 1 h after the addition of 1.0−5.0 mM DTT, and (J) L269C disulfide cross-linked F-actin in the presence of an equimolar amount of phalloidin. The scale bar represents 250 nm.

normally enable RhPh to bind to actin (*14*). Notable, also, is the slower binding of RhPh to un-cross-linked L267C and L269C F-actin than to the other actins. This can be explained by the slightly increased amount of G-actin in the supernatant after pelleting of these mutants, as L267C and L269C are marginally less stable than S265C and V266C. This may also reflect a possible decrease in the filament dynamics and the degree of structural breathing of the L267C and L269C actins.

Site-Directed Spin Labeling. The disulfide cross-linking rate is a function of distance between the cysteines, their p*K*'s in the structure, and the flexibility of the sequences in which they reside (*15*). On the other hand, the magnetic dipolar interaction between spin-labels is a function of interspin distance only. Therefore, SDSL with doubly labeled actins was used to obtain a quantitative evaluation of the distance between C374 and the loop residues.

The nitroxide side chain R1 was introduced at cysteine residues in mutant actins as described in Materials and Methods. Specifically, for the four mutants that were studied, one R1 side chain was introduced at the native C374 and a second at one of the four cysteines introduced along the hydrophobic loop. If the nitroxides in these pairs are less than ~20 Å apart, they interact via a magnetic dipolar interaction that is evident as a broadening of the EPR spectrum. The often subtle broadening due to the magnetic interaction is detected by comparing the EPR spectrum of the doubly labeled protein with a spectrum obtained by reaction with a mixture of spin-label and diamagnetic spin-

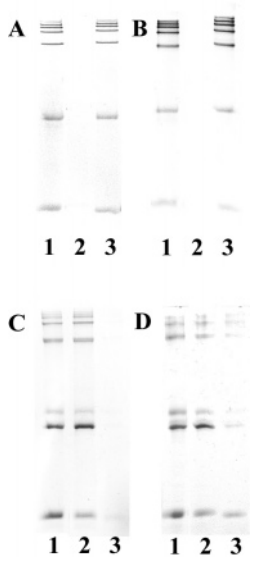

FIGURE 4: Pelleting assays in which actin was subjected to a 360000*g*, 30 min centrifugation to pellet any F-actin present in solution. Lane 1 in each section contained actin just before centrifugation. Lanes 2 and 3 contained samples taken from the supernatant and pellet fractions taken after the high-speed centrifugation, respectively. (A) Disulfide cross-linked S265C. (B) Disulfide cross-linked V266C. (C) Disulfide cross-linked L267C. (D) Disulfide cross-linked L269C. It should be noted that the uncross-linked S265C, V266C, L267C, L269C, S265C/C374A, V266C/C374A, L267C/C374A, and L269C/C374A mutants could be all pelleted, though the L267C/C374A and L269C/C374A mutants less well than the others.

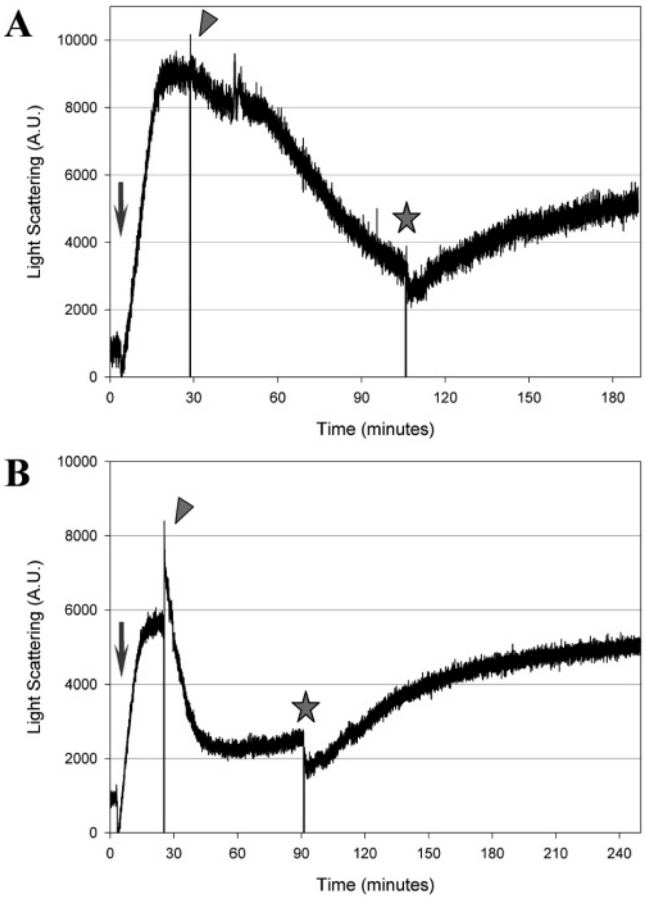

FIGURE 5: Light scattering experiments showing the progression from G- to F-actin (10 μM actin, 2.0 mM $MgCl_2$ to polymerize), the subsequent addition of 30 μM $CuSO_4$ to initiate disulfide cross-linking, and the final addition of DTT (1.0−5.0 mM) to reduce disulfide cross-links. S265C and V266C exhibit no change in light scattering for the duration of cross-linking (not shown). L267C (A) and L269C (B) polymerize normally, but filaments are destroyed with the formation of disulfide cross-links. DTT reduces the cross-links and slowly restores F-actin. Arrows denote the point at which $MgCl_2$ was added. Arrowheads denote the point at which $CuSO_4$ was added. Stars denote the point at which DTT was added.

label analogue, thus representing the line shape in the absence of dipolar interaction (noninteracting reference spectrum). Deconvolution of the two spectra provides a broadening function that can be quantitatively analyzed in terms of interspin distance (*8*, *11*).

In G-actin, the spectrum of each doubly labeled protein is identical with the noninteracting reference spectrum (not shown). Thus, there is no spectral broadening associated with the presence of the spin pair, and the spins must be separated by more than ~20 Å. This is not the case in F-actin, as shown in the normalized spectra of Figure 7. For each case, the spectrum of the doubly labeled mutant (red trace) is compared with the noninteracting reference spectrum (black traces); it is evident that these spectra are different, primarily in the lower amplitude of the doubly labeled protein, reflecting broadening due to dipolar interactions.

Quantitative analysis of the spectra according to the method of Altenbach et al. (*8*) reveals that only ~50% of the nitroxides in the samples have dipolar interactions, presumably due to substoichiometric labeling of the cysteine population with the small excess of reagent (1.5-fold) and short reaction times (1 h) employed. Although this does not complicate the quantitative analysis, the presence of a significant amount of noninteracting nitroxide reduces the apparent magnitude of the dipolar interaction effect. That is, the actual effect is larger than it appears in the spectra of Figure 7. Nevertheless, it is apparent that the strongest interaction is observed for 265R1/374R1, corresponding to interspin distances for the interacting pairs distributed in the range of 12−18 Å. Given the spin probe size and possible motions, this distance distribution may be shifted by another ±5 Å for the relevant cysteine residues. For the other pairs, the interaction is weaker, apparently decreasing in strength from 266R1/374R1 (14−20 Å, ±5 Å) to 267R1/374R1 and 269R1/374R1, with interspin distances distributed near the limit of the SDSL method (≥20 Å).

The EPR spectra of the singly-labeled actin mutants S265R1/C374A, V266R1/C374A, L267R1/C374A, L269R1/C374A, and C374R1 (Figure 8) were used to investigate local dynamics and structural constraints in both G- and F-actin. For interpretation of EPR spectra in terms of nitroxide mobility, the reader is referred to Columbus and Hubbell (*16*), Crane et al. (*17*), and Kusnetzow et al. (*18*). The spectrum of 265R1 in G-actin (green trace) is dominated by a component corresponding to a state of the nitroxide side chain with anisotropic motion characteristic of R1 at solvent-exposed surfaces where the nitroxide has little or no interaction with the protein environment (*16*, *19*). On the other hand, the spectra of 266R1, 267R1, and 269R1 in G-actin are complex, consisting of at least two components corresponding to states of the nitroxide qualitatively described as "mobile" (m) and "immobile" (i) (arrows, Figure 8B−D). The two states could arise from two conformations of the loop in slow exchange on the EPR time scale, one of which is significantly flexible and the other of which is folded in a structure where the nitroxide is involved in tertiary contacts that restrict its motion. However, the two states could also arise from two rotamers of the side chain (*20*). It is interesting to note that the fraction of the more mobile state decreases regularly from 265R1 (≈100%) to 269R1. In terms of either model for the origin of the two states, this implies that the environment around the loop becomes progressively more crowded as one proceeds from residue 265 to 269, providing more opportunity for interaction of the nitroxide.

Upon formation of F-actin, there is only a subtle change in the spectrum of 265R1 (red trace), reflecting a small increase in the degree of ordering of the nitroxide (*19*). The spectral change at 266R1 indicates a modest decrease in mobility for both the i and m components, reflecting new constraints on the motion of R1. For both 265R1 and 266R1, the changes could arise from a damping of backbone motions (*16*). In contrast, both 267R1 and 269R1 become strongly immobilized [the result for 269R1 has been reported (*9*)]. The strong immobilization could arise only from extensive interactions of the nitroxide with the local environment; i.e., the nitroxide is "buried" in the filament structure. Collectively, these results indicate a change in going from G- to F-actin in which an increasing degree of constraints is imposed on R1 along the sequence of residues 265−269. The 374R1 spectra are also composed of two components and exhibit many of the same features as the singly labeled loop residue spectra. When one changes from G- to F-actin, the mobile and immobile components both display a modest decrease in mobility (Figure 8E).

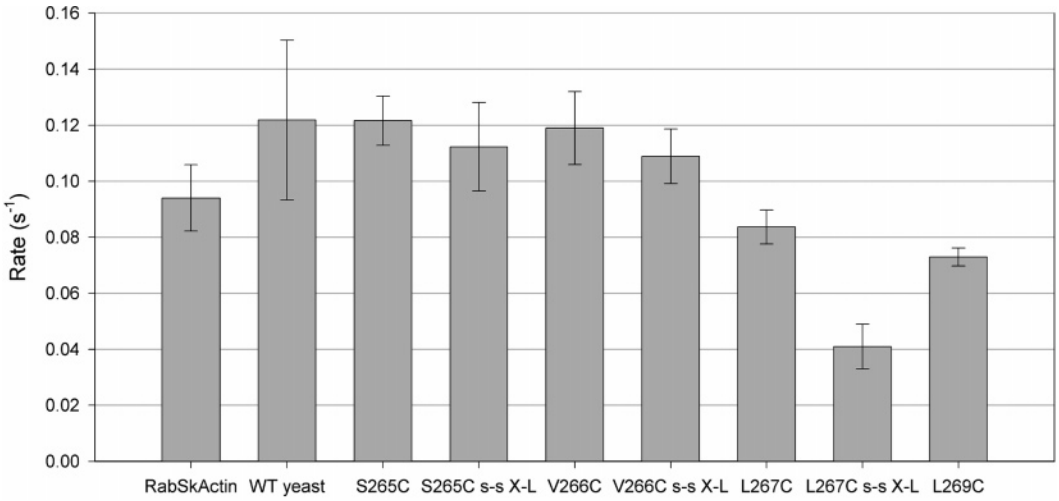

FIGURE 6: Rhodamine−phalloidin binding. Rhodamine-labeled phalloidin (RhPh) was added to disulfide cross-linked and uncross-linked F-actin at a 1:100 RhPh:actin ratio. Cross-linked L269C did not bind RhPh, most likely due to total filament destruction (data not shown). Actin was present at a concentration of 5.0 μM. Error bars represent ± one standard deviation.

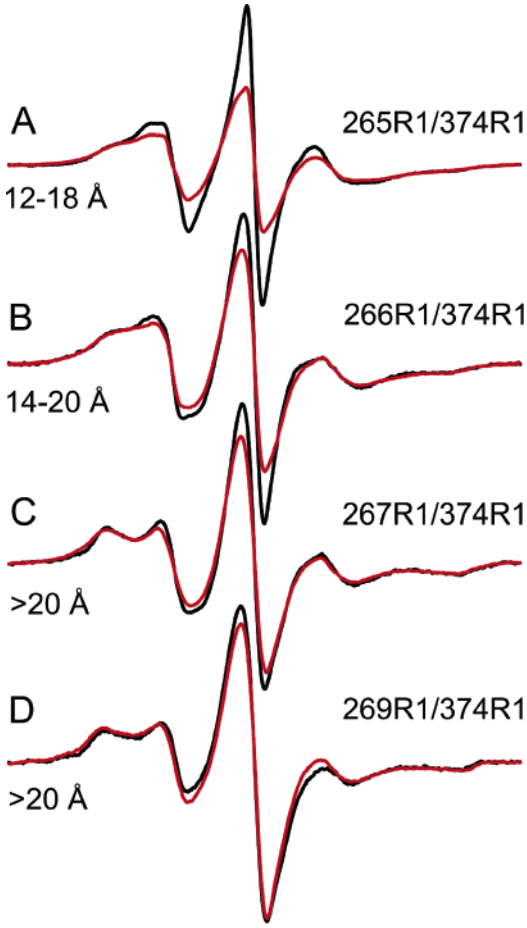

FIGURE 7: EPR spectra of doubly labeled yeast F-actin mutants: (A) 265R1/374R1, 54% interacting; (B) 266R1/374R1, 42% interacting; (C) 267R1/374R1, 0% interacting; and (D) 269R1/374R1, 0% interacting. Black lines depict spectra observed for a mixture of paramagnetically and diamagnetically labeled actin. Red lines depict spectra observed for fully paramagnetically labeled actin. The displayed field range is 100 G.

The presence of F-actin for all mutant spin-labeled actins was verified by electron microscopy (data not shown). It should also be noted that the S265C/C374A, V266C/C374A, L267C/C374A, and L269C/C374A mutants formed normal polymers (data not shown), as observed through light

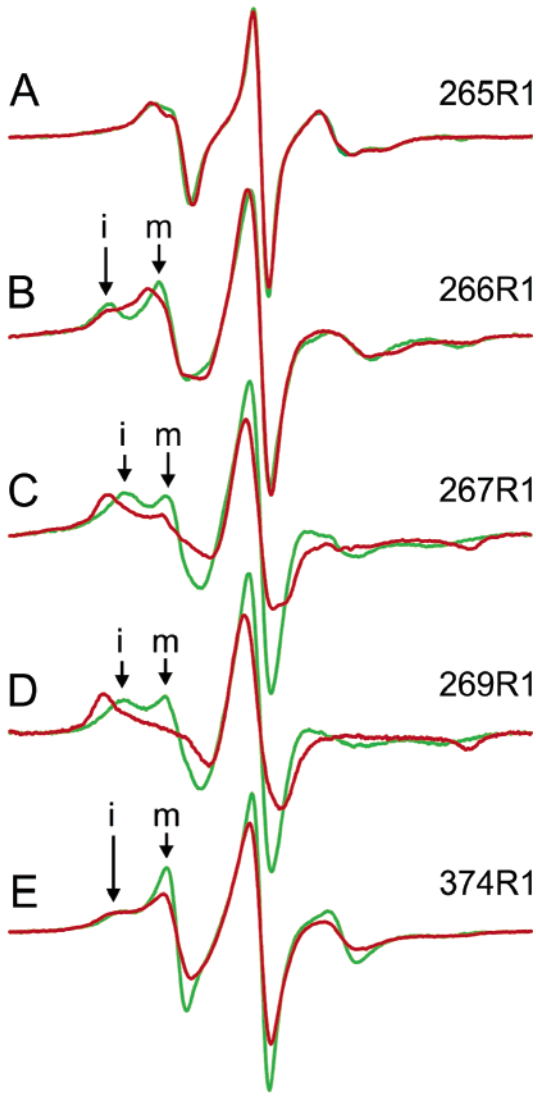

FIGURE 8: EPR spectra of singly labeled yeast wild type and actin double mutants in G- and F-actin: (A) 265R1, (B) 266R1, (C) 267R1, (D) 269R1, and (E) wild type (374R1). Green lines depict G-actin spectra. Red lines depict F-actin spectra. Immobile components in the spectra are designated i, while mobile components are designated m. The displayed field range is 100 G.

scattering and pelleting, though the L267C/C374A and L269C/C374A mutants were polymerized less extensively.

DISCUSSION

The focus of this study was to examine the polymerization-dependent dynamics of the hydrophobic loop (residues 262−274) of actin using a combination of disulfide cross-linking, EPR spectroscopy, and electron microscopy methods. For these studies, we used four yeast actin mutants in which hydrophobic residues at positions 265−267 and 269 were replaced with cysteines, enabling cross-linking and labeling with EPR reagents. The hypothesis of the original Holmes model of the actin filament was that upon polymerization, this loop extended from its parked position along the actin monomer (*2*). The result of the Holmes model was that the hydrophobic plug at the tip of the loop inserted into a hydrophobic pocket formed by the interface of two actin protomers on the opposing strand of the actin filament. This insertion would result in cross-strand stabilization of the filament. In the Holmes model, L267 of the loop lies closest to C374 on a protomer across the interstrand space with V266, S265, and L269 being increasingly distant from C374.

Taken together, the results of our disulfide cross-linking, EPR studies, and solution experiments, however, do not agree with the predictions of the Holmes model (*2*). Our data demonstrate that the position of the loop in F-actin is more consistent with the parked rather than the extended position. In terms of the distance to C374, S265 is closest, followed by V266, L267, and L269. These results do not exclude the possibility of loop extension in a dynamic sense, but the broad interspin distance distributions and the cross-linking studies together strongly favor a situation in which the loop populates a range of conformational states within the filament, including those that lead to filament destabilization. It is possible that filament-destabilizing proteins, such as ADF/cofilin, bind and capture protomers while they are sampling these less energetically favorable states. Importantly, the extent of cross-linking does not indicate the extent to which these less favorable states are being sampled since the cross-linking reaction may be pulling the equilibria that dictate the relative population of these states at any one time.

Insights into the dynamics of the loop provided by our results are particularly interesting. The EPR data show that actin polymerization results in a substantially decreased mobility for probes at positions 267 and 269 (Figure 8), a smaller decrease for a probe at position 266, and little change in mobility at position 265, as if the loop were rotating in a way that sequestered positions 267 and 269 and kept position 265 exposed. This interpretation also correlates with the cross-linking data in two aspects. First, there is easier cross-linking between residues C265 and C266 with C374 on the opposing strand than there is with C267 and C269; second, cross-links with the first two positions do not destabilize filaments, whereas cross-linking with the second pair of residues results in filament disruption. Phalloidin, which stabilizes actin filaments (*13*), actually accelerates cross-linking of C374 to either cysteine at position 265 or 266. However, phalloidin inhibits cross-linking to the other two residues by restricting the flexibility and dynamics of the filament in a manner that confines these other two residues to energetically more favorable sequestered states. In agreement with this interpretation are the results of a previous study in which we cross-linked the loop to the surface of the G-actin monomer (*3*). In this case, polymerization was prevented by covalently freezing the loop into a less favorable conformation such that polymerization could not even be rescued by phalloidin. Thus, there appears to be a line of transition within the loop, with the two parts of the loop on the two sides of this line exhibiting different behavior during actin polymerization. One might speculate that the loop is able to twist at the V266−L267 border in such a way that half of the loop (including residues S265 and V266) is left in a more mobile state, whereas residues on the other half of the loop (including residues L267 and L269) become more buried and less mobile. EPR spectra for C267 and C269 reveal the presence of two components, which indicates the probes reside in two states, one minor and mobile and one major and immobile (Figure 7C,D). Furthermore, molecular modeling of the spin-labeled actin filament revealed that the immobilization measured experimentally is consistent with the parked F-actin (*21*) and new dimer F-actin (*22*) models, but not with the extended model of the actin filament (data not shown). The extended loop model would require that S265 and V266 be relatively immobile, which is in conflict with our results.

Our results are in general agreement with previous studies with these mutants in which the behavior of fluorescent probes attached to each of the hydrophobic plug residues was determined (*6*). First, pyrenes attached to position 265 or 266 formed excimer bands caused by overlap with a pyrene at C374 on a protomer in the opposite strand. No such bands were seen with probes at position 267 or 269. Formation of such overlap requires that the cysteines to which the probes are attached be less that 20 Å apart, in agreement with our EPR studies. Moreover, on the basis of the fact that pyrenes at residue 266 or 267 did not interfere with polymerization, Musib et al. (*6*) argued that it was not necessary for the loop to be stably extended for polymer formation since there is no room in the extended loop model to accommodate the bulky pyrene probe at these positions. Finally, the behavior of the pyrene at each of the loop sites during polymerization was also in agreement with our results. The fluorescence of probes at residues 267 and 269 increased during polymerization, while those at residues 265 and 266 decreased, suggesting an unparking and rotation of the loop much like that predicted here by our cross-linking and EPR studies.

Our work clearly demonstrates the importance of the dynamics of the hydrophobic loop in actin polymerization. Results from the earlier studies using pyrene probes might be somewhat suspect due to the bulky hydrophobic nature of the probe, which may have significantly altered actin filament behavior. Our use of zero-length cross-linking and much smaller sized probes, coupled with EPR, reinforces the earlier findings, and the determination of cross-linking rates and the interprobe distances determined by EPR places the analysis of hydrophobic loop behavior on a much more quantitative footing. The collective weight of self-consistent evidence obtained in this work from such different approaches, and the consideration of prior studies, have helped to illuminate the average conformational state of the hydrophobic loop within the actin filament and also to establish a system where the effects on actin filament structure by

various filament-stabilizing and -destabilizing proteins can be better assessed.

ACKNOWLEDGMENT

We thank Dr. Kálmán Hideg for his generous gift of methanethiosulfonate reagents used in SDSL experiments.

REFERENCES

1. Salwinski, L., Miller, C. S., Smith, A. J., Pettit, F. K., Bowie, J. U., and Eisenberg, D. (2004) The Database of Interacting Proteins: 2004 Update, *Nucleic Acids Res. 32*, D449−D451.
2. Holmes, K. C., Popp, D., Gebhard, W., and Kabsch, W. (1990) Atomic Model of the Actin Filament, *Nature 347*, 44−49.
3. Shvetsov, A., Musib, R., Phillips, M., Rubenstein, P. A., and Reisler, E. (2002) Locking the Hydrophobic Loop 262−274 to G-Actin Surface by a Disulfide Bridge Prevents Filament Formation, *Biochemistry 41*, 10787−10793.
4. Orlova, A., Shvetsov, A., Galkin, V. E., Kudryashov, D. S., Rubenstein, P. A., Egelman, E. H., and Reisler, E. (2004) Actin-Destabilizing Factors Disrupt Filaments by Means of a Time Reversal of Polymerization, *Proc. Natl. Acad. Sci. U.S.A. 101*, 17644−17648.
5. Feng, L., Kim, E., Lee, W. L., Miller, C. J., Kuang, B., Reisler, E., and Rubenstein, A. (1997) Fluorescence Probing of Yeast Actin Subdomain 3/4 Hydrophobic Loop 262-274, Actin-Actin and Actin-Myosin Interactions in Actin Filaments, *J. Biol. Chem. 272*, 16829−16837.
6. Musib, R., Wang, G., Geng, L., and Rubenstein, P. A. (2002) Effect of Polymerization on the Subdomain 3/4 Loop of Yeast Actin, *J. Biol. Chem. 277*, 22699−22709.
7. Kim, E., Wriggers, W., Phillips, M., Kokabi, K., Rubenstein, P. A., and Reisler, E. (2000) Cross-Linking Constraints on F-Actin Structure, *J. Mol. Biol. 299*, 421−429.
8. Altenbach, C., Oh, K. J., Trabanino, R. J., Hideg, K., and Hubbell, W. L. (2001) Estimation of Inter-Residue Distances in Spin Labeled Proteins at Physiological Temperatures: Experimental Strategies and Practical Limitations, *Biochemistry 40*, 15471−15482.
9. Shvetsov, A., Stamm, J. D., Phillips, M., Warshaviak, D., Altenbach, C., Rubenstein, P. A., Hideg, K., Hubbell, W. L., and Reisler, E. (2006) Conformational Dynamics of Loop 262-274 in G- and F-actin, *Biochemistry 45*, 6541−6549.
10. Hubbell, W. L., Froncisz, W., and Hyde, J. S. (1987) Continuous and Stopped Flow EPR Spectrometer Based on a Loop Gap Resonator, *Rev. Sci. Instrum. 58*, 1879−1886.
11. Rabenstein, M. D., and Shin, Y. K. (1995) Determination of the Distance Between Two Spin Labels Attached to a Macromolecule, *Proc. Natl. Acad. Sci. U.S.A. 92*, 8239−8243.
12. Pake, G. (1948) Nuclear Resonance Absorption in Hydrated Crystals: Fine Structure of the Proton Line, *J. Chem. Phys. 16*, 327−336.
13. Dancker, P., Low, I., Hasselbach, W., and Wieland, T. (1975) Interaction of Actin with Phalloidin: Polymerization and Stabilization of F-actin, *Biochim. Biophys. Acta 400*, 407−414.
14. De La Cruz, E. M., and Pollard, T. (1994) Transient Kinetic Analysis of Rhodamine Phalloidin Binding to Actin Filaments, *Biochemistry 33*, 14387−14392.
15. Hubbell, W. L., Altenbach, C., Hubbell, C. M., and Khorana, H. G. (2003) Rhodopsin Structure, Dynamics, and Activation: A Perspective from Crystallography, Site-Directed Spin Labeling, Sulfhydryl Reactivity, and Disulfide Cross-Linking, *Adv. Protein Chem. 63*, 243−290.
16. Columbus, L., and Hubbell, W. L. (2002) A New Spin on Protein Dynamics, *Trends Biochim. Sci. 27*, 288−295.
17. Crane, J. M., Mao, C., Lilly, A. A., Smith, V. F., Suo, Y., Hubbell, W. L., and Randall, L. L. (2005) Mapping of the Docking of SecA onto the Chaperone SecB by Site-Directed Spin Labeling: Insight into the Mechanism of Ligand Transfer During Protein Export, *J. Mol. Biol. 353*, 295−307.
18. Kusnetzow, A. K., Altenbach, C., and Hubbell, W. L. (2006) Conformational States and Dynamics of Rhodopsin in Micelles and Bilayers, *Biochemistry 45*, 5538−5550.
19. Columbus, L., Kalai, T., Jeko, J., Hideg, K., and Hubbell, W. L. (2001) Molecular Motion of Spin Labeled Side Chains in α-Helices: Analysis by Variation of Side Chain Structure, *Biochemistry 40*, 3828−3846.
20. Langen, R., Oh, K. J., Cascio, D., and Hubbell, W. L. (2000) Crystal Structures of Spin Labeled T4 Lysozyme Mutants: Implications for the Interpretation of EPR Spectra in Terms of Structure, *Biochemistry 39*, 8396−8405.
21. Holmes, K. C., Angert, I., Kull, F. J., Jahn, W., and Schroder, R. R. (2003) Electron Cryo-Microscopy Shows how Strong Binding of Myosin to Actin Releases Nucleotide, *Nature 425*, 423−427.
22. Kudryashov, D. S., Sawaya, M. R., Adisetiyo, H., Norcross, T., Hegyi, G., Reisler, E., and Yeates, T. O. (2005) The Crystal Structure of a Cross-Linked Actin Dimer Suggests a Detailed Molecular Interface in F-actin, *Proc. Natl. Acad. Sci. U.S.A. 102*, 13105−13110.

BI061229F